



**MODELING OF PROOF MASS SELF-GRAVITY FIELD FOR
THE LASER INTERFEROMETRY SPACE ANTENNA (LISA)**

Marco B. Quadrelli

**14th AAS/AIAA Space Flight
Mechanics Conference**

Maui, Hawaii,

February 8-12, 2004

MODELING OF PROOF MASS SELF-GRAVITY FIELD FOR THE LASER INTERFEROMETRY SPACE ANTENNA (LISA)¹

Marco B. Quadrelli²

This paper describes the development of the self-gravity modeling tool used to predict and control the motion of one of the proof masses of the orbiting LISA gravitational wave detector. LISA is a space-borne gravitational wave detector, which is formed by three spacecraft orbiting the Sun and forming the vertices of an equilateral triangle with a side of 5 million km in length. Requirements on the forces and moments, and the force gradients and moment gradients, applied to the proof mass exist. This paper computes these quantities analytically, so that gravitational balancing considerations can now be done effectively.

Introduction

This paper describes the development of the self-gravity tool used to predict and control the motion of one of the proof masses of the orbiting LISA gravitational wave detector. LISA is a space-borne gravitational wave detector, which is formed by three spacecraft orbiting the Sun and forming the vertices of an equilateral triangle with a side of 5 million km in length. Inside each spacecraft, shown in Figure 1, an optical bench monitors the motion of two separated proof masses, which reflect the laser light from the adjacent spacecraft along the edges of the equilateral triangle, and senses the gravitational wave signal with unprecedented sensitivity.

A modeling challenge described in the paper is how to consider the distributed force and torque between all the participating extended bodies. Gravitational forces and moments on each extended body are computed exactly from the closed form expression of the gravitational potential of a parallelepiped. This approach is currently being incorporated into a general finite element-based self-gravity computational tool at JPL for the LISA spacecraft. Requirements on the forces and moments, and the force gradients and moment gradients, applied to the proof mass exist, therefore these quantities must be computed independently.

¹ Copyright © 2004 by The American Astronautical Society.

² M.S. 198-326, Jet Propulsion Laboratory, California Institute of Technology, 4800 Oak Grove Drive, Pasadena, CA 91109, marco@grover.jpl.nasa.gov

The performance of the Self-Gravity Tool (SGT) has implications out flowing into the ACS, and into the Disturbance Rejection System. For example, we need to be able to address gravity trimming scenarios arising when the telescope articulation is moving, or issues like mass depletion from several sources, including thermal disturbances. Figure 1 shows the essential functionality needed by a general multibody self-gravity analysis tool:

- capability to handle multiple moving bodies of arbitrary geometry, attitude, and location
- capability to handle gravitational interaction in close proximity between extended bodies
- capability to reconstruct the gravitational interaction from sub-bodies up to the entire system
- capability to dynamically vary the topology of the system by moving, adding, and removing bodies.

The computational self-gravity tool described in this paper supports a multibody grid of extended bodies possibly of non-homogeneous densities (example body-grids are point masses and generic parallelepipeds located at arbitrary locations and attitudes around the LISA proof mass). Bodies can be fixed, moving around the proof mass, or deformed under thermoelastic loads. The self-gravity potential calculation is exact (i.e. no order expansions of the potential are involved) up to the gradients of forces and moments.

At JPL, we have developed several codes and interfaces to those codes. The intent was to provide a variety of tools using different methods to approach the same problem. That way, independent validation analyses can be done. So far we have developed:

- 1) **SGT Tool 1:** A self-gravity modeling tool using only second order expansions of the force and gradients, for initial self-gravity estimation [1] and for preliminary dynamic simulation.
- 2) **SGT Tool 2:** A self-gravity modeling tool using only a mesh of points, and a summation over all points [1].
- 3) **SGT Tool 3:** A self-gravity modeling tool using an exact representation of the gravitational potential around the proof mass, and either a summation over known nodal locations or a higher-order Gauss-Legendre integration over all elements surrounding the proof mass that are part of a finite element mesh [2].

In the following, we will summarize the approach of each method.

Steps for a General Calculation of the Interacting Fields between Extended Bodies

Figure 2 depicts the geometry of the problem, and the potential of the gravitational interaction between an extended three-dimensional parallelepiped and a point mass source, located at x . Here, the proof mass, or a sub-element of it shaped as a parallelepiped, interacts gravitationally with the point source mass M . Any arbitrary mass distribution surrounding the proof mass can be thus computed by combining the effects of each point mass individually. Denote the distance between these two mass elements by r , so that r represents the distance between the origins of the two extended bodies “proof mass” and “source body M ” (Figure 2). The gravitational potential due to the interaction is

$$V=V(\mathbf{r})=GMm|\mathbf{r}|^{-1} \tag{1}$$

Let us vary the kinematics of the parallelepiped B , keeping the source M fixed, and assuming only small rotations:

$$\delta \mathbf{r} = -\delta^o \mathbf{r} + (\mathbf{r} \times \mathbf{1}) \cdot \delta \boldsymbol{\theta} \quad (2)$$

where we use the $(\bullet) \times \mathbf{1}$ operator for the skew-symmetric operator applied to a vector, and $\delta^o(\bullet)$ for the variation of a vector taken in the intrinsic (body-fixed) frame.

The virtual variation of the potential becomes:

$$\delta V = \frac{\partial V}{\partial \mathbf{r}} \cdot \delta^o \mathbf{r} + \left(\mathbf{r} \times \frac{\partial V}{\partial \mathbf{r}} \right) \cdot \delta \boldsymbol{\theta} \quad (3)$$

Consequently, the forces and moments, and the forces and moment gradients originate from the variation of the potential as follows:

$$\begin{aligned} F &= \frac{\partial V}{\partial \mathbf{r}} \\ M &= \mathbf{r} \times \frac{\partial V}{\partial \mathbf{r}} \end{aligned} \quad (4)$$

$$\begin{pmatrix} \delta \mathbf{F} \\ \delta \mathbf{M} \end{pmatrix} = \begin{bmatrix} \frac{\partial V}{\partial^o \mathbf{r} \partial^o \mathbf{r}} & \mathbf{r} \times \frac{\partial V}{\partial^o \mathbf{r} \partial^o \mathbf{r}} \\ \frac{\partial \mathbf{M}}{\partial(\partial^o \mathbf{r})} & \frac{\partial \mathbf{M}}{\partial(\partial \boldsymbol{\theta})} \end{bmatrix} \begin{pmatrix} \delta^o \mathbf{r} \\ \delta \boldsymbol{\theta} \end{pmatrix} \quad (5)$$

$$\frac{\partial \mathbf{M}}{\partial(\partial^o \mathbf{r})} = \mathbf{E}_1 - \mathbf{F} \times \mathbf{U} \quad (6)$$

$$\frac{\partial \mathbf{M}}{\partial(\partial \boldsymbol{\theta})} = (\mathbf{r} \otimes \mathbf{F}) - (\mathbf{F} \cdot \mathbf{r}) \mathbf{U} - \mathbf{E}_2 \quad (7)$$

where the symbol \otimes represents outer product, and with the following definitions:

$$\mathbf{r} \times \left(\frac{\partial F}{\partial^o \mathbf{r}} \cdot \partial^o \mathbf{r} \right) = \mathbf{E}_1 \partial^o \mathbf{r} \quad (8)$$

$$\mathbf{r} \times \left[\frac{\partial F}{\partial \mathbf{r}} \cdot (\mathbf{r} \times \partial \theta) \right] = \mathbf{E}_2 \partial \theta \quad (9)$$

The last step is to sum over all points x of any extended body around the proof mass parallelepiped. This can be done either by summing over a (very) large number of points, or by integrating over finite elements of irregular shapes at the Gauss-Legendre nodes. The equations above represent a coordinate-free representation of the field action and its spatial gradients between interacting mass points.

Figure 3 shows the computed bounds below which one can consider an adjacent extended body as a point mass with respect to the proof mass. Figure 4 shows the initial mesh used for predicting the gravitational interaction between two extended cubes. The methods used for modeling the gravitational field and its gradients are: 1) by summing the gravitational forces and gradients after discretization of the source mass into a large number of mass points, (Figure 5), and 2) by summing the gravitational forces and gradients after discretization of the source mass into a much smaller number of Gauss-Legendre points (Figure 6). The conclusion is that very few, optimally located Gauss-Legendre points (4 points along each side of the cube, in the example of Figure 3) achieve the same result (accuracy of force prediction within 0.5% of exact value) than more than 5000 points into which the source cube is discretized. This result is extremely convenient for analyses using a dynamic gravitational field, and gravitational balancing considerations can now be done effectively. A second paper applies some of these models to the gravitational dynamic control of the displacement of the proof mass.

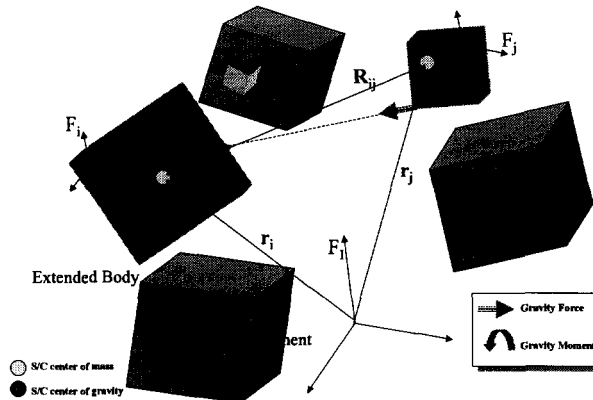


Figure 1. Multibody gravitational modeling elements.

SGT TOOL 1: Potential, Forces, and Gradients with 2nd Order Method

Given a dynamically deformed set of nodes $[xyz]$ (caused by thermal deformation or dynamical vibration), the finite element mass matrix $[M]$, and the array of nodal degrees of freedom and connectivity, this tool provides the matrix

$$\mathbf{M} = \begin{bmatrix} \mathbf{m} & \tilde{\mathbf{c}} \\ -\tilde{\mathbf{c}} & \mathbf{J} \end{bmatrix} \quad (10)$$

and the location of the center of mass using the rigid body modes, for each extended body. Here, \mathbf{m} and \mathbf{J} are the mass and moment of inertia matrices of the (possibly deformed) extended body about its own center of mass, and \mathbf{c} is the vector of the first moment of inertia. The tilde operator above a symbol denotes the skew-symmetric matrix associated with that symbol. The computational approach is as follows:

- 1) Once the location of the center of mass, nodal distribution, and mass properties of each (deformed) extended body are known,
- 2) Establish the visibility map for the set of bodies (should be full, maybe sparse if the analyst is interested in proximity effects only). May not need all bodies.
- 3) Compute resultant gravity force for each extended body.
- 4) Compute center of gravity of each extended body.
- 5) Compute resultant gravity torque about center of mass of each body.

To map the interaction between multiple extended bodies, we have introduced the concept of the visibility map [3]. See Figure 2. V_m is the VISIBILITY MAP. In components, it is given by $\{a_{ij}\}$ from body (or mesh) Φ_i to body (or mesh) Φ_j . It allows the analyst to include or neglect mass distribution.

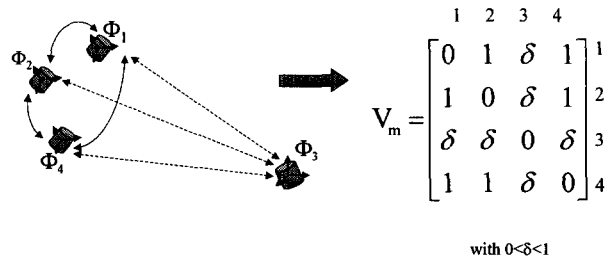


Figure 2. Visibility map.

For the two cube problem, the inertia dyadic for cubes of side s is given by $I = (m_i s_i^2 / 6)(\mathbf{b}_1 \mathbf{b}_1 + \mathbf{b}_2 \mathbf{b}_2 + \mathbf{b}_3 \mathbf{b}_3)$ and $J = (m_j s_j^2 / 6)(\mathbf{b}_1 \mathbf{b}_1 + \mathbf{b}_2 \mathbf{b}_2 + \mathbf{b}_3 \mathbf{b}_3)$. The gravitational force on body i from body j , to 2nd order can be derived as [1]:

$$\mathbf{F}_{ij} = -(Gm_i m_j / R_{ij}^2)(\mathbf{a}_i + \mathbf{f}_i + \mathbf{g}_j) \quad (11)$$

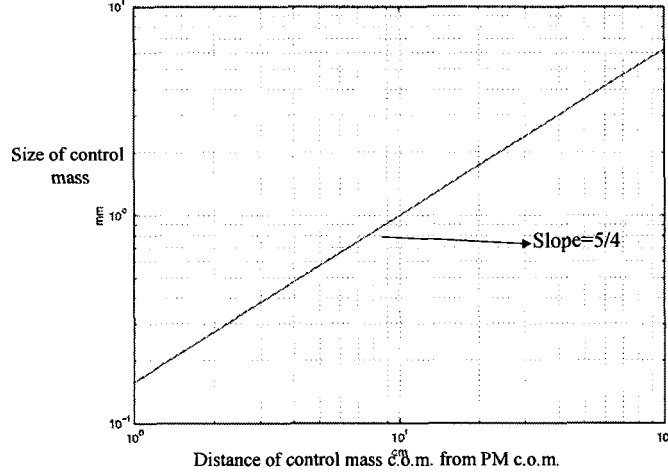
where

$$\mathbf{f}_i = (1/m_i R_{ij}^2) \{ (3/2) [\text{trace}(\mathbf{I}) - 5 \mathbf{a}_i \cdot \mathbf{I} \mathbf{a}_i] \mathbf{a}_i + 3 \mathbf{I} \mathbf{a}_i \} \quad (12)$$

$$\mathbf{g}_j = (1/m_j R_{ij}^2) \{ (3/2) [\text{trace}(\mathbf{J}) - 5 \mathbf{a}_i \cdot \mathbf{J} \mathbf{a}_i] \mathbf{a}_i + 3 \mathbf{J} \mathbf{a}_i \} \quad (13)$$

and similarly for body j . We now introduce the rotation tensor \mathbf{C} for body i , with components $C_{mn} = i_m \mathbf{b}_n$.

Simplifying, after having introduced the components of \mathbf{a}_1 in the inertial frame in terms of the two angles θ and ϕ . Therefore, body j acts on body i , as a point mass within an accuracy of ϵ , when $s_j < [\epsilon R_{ij}^4 / (6Gm_j \rho_1 \cos \theta \cos \phi)]^{1/5}$ (for the force along x , for instance). We have taken $\epsilon = 10^{-15}$. Figure 3 shows the



result.

Figure 3. At what distance from the proof mass can a cube be approximated by a point.

The gravitational force gradient on body i from body j , to 2nd order:

$$d\mathbf{F}_i/d\mathbf{R}_{ij} = -(Gm_i m_j / R_{ij}^3)(1 - 3 \mathbf{a}_1 \otimes \mathbf{a}_1) + (3Gm_i / 2R_{ij}^5) \mathbf{H}_i + (3Gm_j / 2R_{ij}^5) \mathbf{H}_j \quad (14)$$

where

$$\mathbf{H}_i = \text{tr}(\mathbf{I})[5(\mathbf{a}_1 \otimes \mathbf{a}_1) - \mathbf{1}] - 2\mathbf{1} + (\mathbf{a}_1 \cdot \mathbf{I} \cdot \mathbf{a}_1)[5\mathbf{1} - 35(\mathbf{a}_1 \otimes \mathbf{a}_1)] + 10 \mathbf{a}_1 (\mathbf{a}_1 \cdot \mathbf{I}) + 10(\mathbf{a}_1 \cdot \mathbf{I}) \mathbf{a}_1 \quad (15)$$

$$\mathbf{H}_j = \text{tr}(\mathbf{J})[5(\mathbf{a}_1 \otimes \mathbf{a}_1) - \mathbf{1}] - 2\mathbf{1} + (\mathbf{a}_1 \cdot \mathbf{J} \cdot \mathbf{a}_1)[5\mathbf{1} - 35(\mathbf{a}_1 \otimes \mathbf{a}_1)] + 10 \mathbf{a}_1 (\mathbf{a}_1 \cdot \mathbf{J}) + 10(\mathbf{a}_1 \cdot \mathbf{J}) \mathbf{a}_1 \quad (16)$$

The center of gravity computation proceeds as follows:

- 1) find potential V and force $\mathbf{F} = -\tilde{\mathbf{N}}_R V$ on body B due to a unit mass at \mathbf{x} ,
- 2) Define vector $\mathbf{v}_x = x(1) \mathbf{b}_1 + x(2) \mathbf{b}_2 + x(3) \mathbf{b}_3$ from center of mass of B to point mass, and calculate the location $R = (Gm_0 m / |\mathbf{F}|)^{1/2}$ of the center of gravity along the con-joining line,
- 3) the location of center of gravity in body frame of extended body B is at $\mathbf{r}_{cg} = \mathbf{v}_x - R\mathbf{u}$.

Finally, we can compute the forces and moments gradients. We compute the gradients over the volume V_0 :

$$\mathbf{F} = \frac{Gm_0}{V_0} \left(\frac{\partial V_a}{\partial \mathbf{x}} + \frac{\partial V_b}{\partial \mathbf{x}} \right) \quad (17)$$

$$\mathbf{G} = \frac{Gm_0}{V_0} \nabla_{\mathbf{x}} \otimes \left(\frac{\partial V_a}{\partial \mathbf{x}} + \frac{\partial V_b}{\partial \mathbf{x}} \right) \quad (18)$$

SGT TOOL 2: Potential, Forces, and Gradients with Mesh Method

See Figure 4. A small mass element m of the proof mass, located at ρ in the proof mass body frame, interacts gravitationally with the source node M . The distance between these two mass elements is: $\mathbf{d} = \mathbf{R} - \mathbf{R}_0 - \rho$. Consequently, the gravitational potential is

$$V = V(\mathbf{r}) = GMm|\mathbf{r}|^{-1} \quad (19)$$

$$|\mathbf{d}|^{-1} = (\mathbf{R} - \mathbf{R}_0)^{-1} \left[1 + \frac{\rho \cdot \rho}{(\mathbf{R} - \mathbf{R}_0)^2} - \frac{2\rho \cdot (\mathbf{R} - \mathbf{R}_0)}{(\mathbf{R} - \mathbf{R}_0)^2} \right]^{-1/2} \quad (20)$$

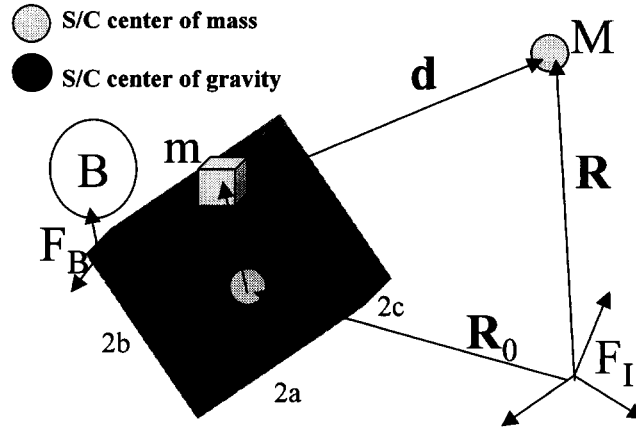


Figure 4. Geometry used for SGT Tool 2.

Denote the term in square brackets by $[\cdot]^{-3/2}$. Now vary the kinematics of the proof mass B, keeping M fixed and assuming only small rotations:

$$\delta \mathbf{d} = -\delta^o \rho + (\rho \times \mathbf{1}) \cdot \delta \theta \quad (21)$$

$$\delta V = \mathbf{F} \cdot \delta^0 \boldsymbol{\rho} + \mathbf{M} \cdot \delta \boldsymbol{\theta} \quad (22)$$

Consequently, the forces and moments, and the forces and moment gradients originate from the variation of the potential as follows:

$$\mathbf{F} = \frac{GmM[\cdot]^{-3/2}}{|R - R_0|^3} \mathbf{d} \quad (23)$$

$$\mathbf{M} = \frac{GmM[\cdot]^{-3/2}}{|R - R_0|^3} (\boldsymbol{\rho} \times \mathbf{d}) \quad (24)$$

$$\begin{pmatrix} \delta \mathbf{F} \\ \delta \mathbf{M} \end{pmatrix} = \begin{bmatrix} \frac{\partial \mathbf{F}}{\partial (\delta^0 \boldsymbol{\rho})} & \frac{\partial \mathbf{F}}{\partial (\delta \boldsymbol{\theta})} \\ \frac{\partial \mathbf{M}}{\partial (\delta^0 \boldsymbol{\rho})} & \frac{\partial \mathbf{M}}{\partial (\delta \boldsymbol{\theta})} \end{bmatrix} \begin{pmatrix} \delta^0 \boldsymbol{\rho} \\ \delta \boldsymbol{\theta} \end{pmatrix} \quad (25)$$

$$\frac{\partial \mathbf{F}}{\partial (\delta \boldsymbol{\theta})} = -\boldsymbol{\rho} \times \frac{\partial \mathbf{F}}{\partial (\delta^0 \boldsymbol{\rho})} \quad (26)$$

$$\frac{\partial \mathbf{M}}{\partial (\delta \boldsymbol{\theta})} = -\boldsymbol{\rho} \times \frac{\partial \mathbf{M}}{\partial (\delta^0 \boldsymbol{\rho})} \quad (27)$$

$$\frac{\partial \mathbf{F}}{\partial (\delta^0 \boldsymbol{\rho})} = \frac{GmM[\cdot]^{-3/2}}{|R - R_0|^3} \left\{ \frac{3[\cdot]^{-1}}{|R - R_0|^2} (\mathbf{d} \otimes \mathbf{d}) - \mathbf{U} \right\} \quad (28)$$

$$\frac{\partial \mathbf{M}}{\partial (\delta^0 \boldsymbol{\rho})} = \frac{GmM [\cdot]^{-3/2}}{|R - R_0|^3} \times \left\{ \frac{3[\cdot]^{-1}}{|R - R_0|^2} [(\boldsymbol{\rho} \times \mathbf{d}) \otimes \mathbf{d}] - [(\mathbf{R} - \mathbf{R}_0) \times \mathbf{U}] \right\} \quad (29)$$

with tensor product $(\mathbf{a} \cdot \mathbf{b})\mathbf{c} = (\mathbf{c} \otimes \mathbf{b})\mathbf{a} = (\mathbf{c} \otimes \mathbf{a})\mathbf{b}$ and unit tensor $\mathbf{U} = \delta_{ij} \mathbf{e}_i \mathbf{e}_j$. As a result, we obtain a coordinate free representation of the forces, moments, force gradients and moment gradients.

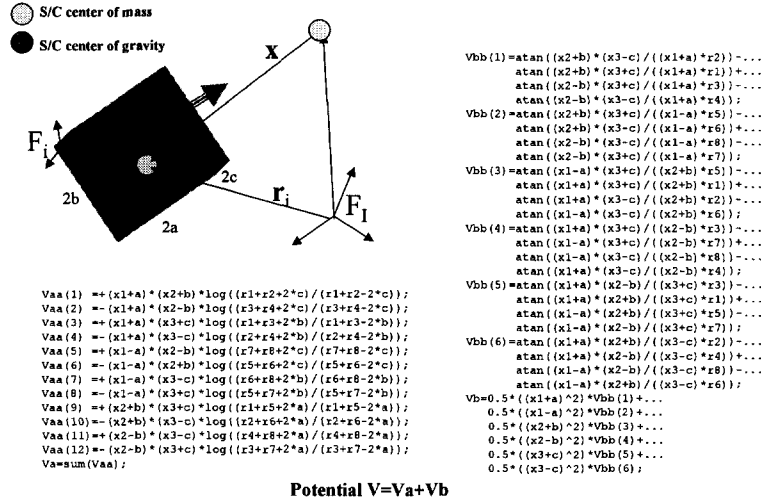


Figure 5. Gravitational Potential of Parallelepiped at x [2].

SGT TOOL 3: Potential, Forces, and Gradients with Exact Extended Body Method

This method similar to the one described in [4]. See Figure 5, where the exact representation on the potential, taken from [4], is also shown. Here, the proof mass, or a sub-element of it shaped as a parallelepiped, interacts gravitationally with the source mass M as before. Denote the distance between these two mass elements by r , where now r represents the distance between the origins of the two extended bodies “proof mass” and “source body M”. The gravitational potential is $V=V(\mathbf{r})=GMm|\mathbf{r}|^{-1}$. Again, let us vary the kinematics of B, keeping M fixed assuming only small rotations:

$$\delta \mathbf{r} = -\delta^o \mathbf{r} + (\mathbf{r} \times \boldsymbol{\theta}) \cdot \delta \boldsymbol{\theta} \quad (30)$$

$$\delta V = \frac{\partial V}{\partial \mathbf{r}} \cdot \delta^0 \mathbf{r} + \left(\mathbf{r} \times \frac{\partial V}{\partial \mathbf{r}} \right) \cdot \delta \boldsymbol{\theta} \quad (31)$$

Consequently, the forces and moments, and the forces and moment gradients originate from the variation of the potential as follows:

$$\begin{aligned} F &= \frac{\partial V}{\partial \mathbf{r}} \\ M &= \mathbf{r} \times \frac{\partial V}{\partial \mathbf{r}} \end{aligned} \quad (32)$$

$$\begin{pmatrix} \delta \mathbf{F} \\ \delta \mathbf{M} \end{pmatrix} = \begin{bmatrix} \frac{\partial V}{\partial^0 \mathbf{r} \partial^0 \mathbf{r}} & \mathbf{r} \times \frac{\partial V}{\partial^0 \mathbf{r} \partial^0 \mathbf{r}} \\ \frac{\partial \mathbf{M}}{\partial (\partial^0 \mathbf{r})} & \frac{\partial \mathbf{M}}{\partial (\partial \boldsymbol{\theta})} \end{bmatrix} \begin{pmatrix} \delta^0 \mathbf{r} \\ \delta \boldsymbol{\theta} \end{pmatrix} \quad (33)$$

$$\frac{\partial \mathbf{M}}{\partial (\partial^0 \mathbf{r})} = \mathbf{E}_1 - \mathbf{F} \times \mathbf{U} \quad (34)$$

$$\frac{\partial \mathbf{M}}{\partial (\partial \boldsymbol{\theta})} = (\mathbf{r} \otimes \mathbf{F}) - (\mathbf{F} \cdot \mathbf{r}) \mathbf{U} - \mathbf{E}_2 \quad (35)$$

with the following definitions:

$$\mathbf{r} \times \left(\frac{\partial F}{\partial^0 \mathbf{r}} \cdot \partial^0 \mathbf{r} \right) = \mathbf{E}_1 \partial^0 \mathbf{r} \quad (36)$$

$$\mathbf{r} \times \left[\frac{\partial F}{\partial^0 \mathbf{r}} \cdot (\mathbf{r} \times \partial \boldsymbol{\theta}) \right] = \mathbf{E}_2 \partial \boldsymbol{\theta} \quad (37)$$

The last step is to sum over all points x of any extended body around the proof mass parallelepiped. This can be done efficiently either by summing over a (very) large number of points, or by integrating over finite elements of irregular shapes at the Gauss-Legendre nodes. Compute gravitational force and torque between specified body 0 (parallelepiped), located at r_0 , and an extended body occupying volume

$[a_1, b_1, a_2, b_2, a_3, b_3]$, of density r , with center of mass located at r_1 .

- 2) Integrate a 3-dimensional array (vector or matrix) of size $m \times n$, using an (ng_1, ng_2, ng_3) -th order Gauss-Legendre integration, in extended volume $[(a_1, b_1), (a_2, b_2), (a_3, b_3)]$. Irregular geometry can be handled integrating over simplex elements.

Results of Numerical Benchmark Tests

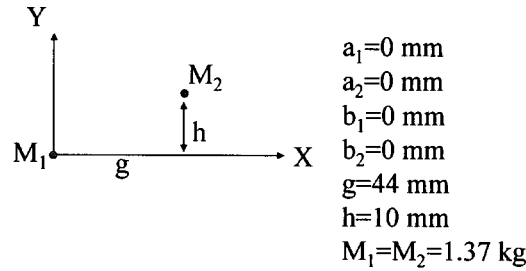
The last two programs (SGT2 and SGT3) have been exercised for some test cases, and the results of the two have been compared. See Figure 6 to Figure 22: Very good agreement between the results of the two codes is shown in these figures. More so, the agreement turned out to improve substantially for the JPL tools when the density of points was increased for the bodies around the primary (proof mass). This improvement came at the expense of a higher computation time.

Figure 6, 7, and 8 shows the comparison between the two results for the cases of two point masses, one cube and a point, and a point and a cube. Figure 9 shows the mesh used for the problem with two cubes, and Figure 11 shows a comparison of the results.

Figure 10 shows a comparison of the results obtained between the point mesh and the extended body mesh for the two cube problem, and these results agree with the trend shown in Figure 3 obtained, however, with only a 2nd order approximation).

Figure 12 shows that a general summation can be used between Gauss points belonging to elements of separated meshes. The result of this high performance computation is shown in Figure 13 and 14, where the axial force (along X) is shown for the two cubes problem as a function of the discretization points (i.e., using SGT2), and using SGT3 (the exact computation), in Figure 14.

Figure 15 and 16 show the results for the case of two long thin bodies placed horizontally, for which an analytical solution exists. Again, the accuracy improved as the mesh in the second body was refined, while the field for the proof mass (primary) was computed using the exact solution. Figure 17 and 18 show the results for the case of two long thin bodies with one placed vertically, for which an analytical solution also exists. Figure 19 shows the agreement of the mesh and exact tools for the case of an infinitely thin ring of radius equal to 1.6 meters, computing the field force when the source unit mass at the center moves laterally.

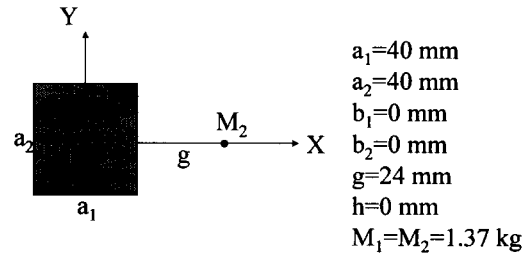


	Point-to-Point			Exact to Point		
Fx (N x 10 ⁻¹⁰) =	599.768			599.863		
Fy (N x 10 ⁻¹⁰) =	136.311			136.732		
Fz (N x 10 ⁻¹⁰) =	0			0		
Mx (Nm x 10 ⁻¹⁰) =	0			0		
My (Nm x 10 ⁻¹⁰) =	0			0		
Mz (Nm x 10 ⁻¹⁰) =	0			0		

	/dx (m)	/dy (m)	/dz (m)	/dx (m)	/dy (m)	/dz (m)
dFx (N/m x 10 ⁻¹⁰) =	25253.7	8837.4	0	25253.6	8827.8	0
dFy (N/m x 10 ⁻¹⁰) =	8837.4	-11622.6	0	8827.8	-11622.5	0
dFz (N/m x 10 ⁻¹⁰) =	0	0	-13631.1	0	0	-13694.4
dMx (Nm/m x 10 ⁻¹⁰) =	0	0	0	0	0	-0.2116
dMy (Nm/m x 10 ⁻¹⁰) =	0	0	0	0	0	2.6907
dMz (Nm/m x 10 ⁻¹⁰) =	0	0	0	-0.8433	0.1916	0

	/dθx (r)	/dθy (r)	/dθz (r)	/dθx (r)	/dθy (r)	/dθz (r)
dFx (N/rad x 10 ⁻¹⁰) =	0	0	136.31	0	0	136.94
dFy (N/rad x 10 ⁻¹⁰) =	0	0	-599.77	0	0	-602.55
dFz (N/rad x 10 ⁻¹⁰) =	-136.31	599.77	0	-135.88	599.67	0
dMx (Nm/rad x 10 ⁻¹⁰) =	0	0	0	-0.00211	0.0093	0
dMy (Nm/rad x 10 ⁻¹⁰) =	0	0	0	0.02690	-0.1183	0
dMz (Nm/rad x 10 ⁻¹⁰) =	0	0	0	0	0	0.01686

Figure 6. Results from benchmark comparison.

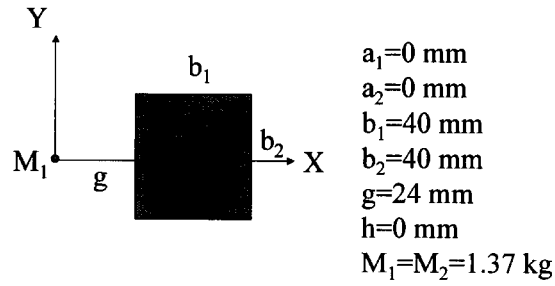


	Point-to-Point			Exact to Point		
Fx (N x 10 ⁻¹⁰) =	620.274			620.274		
Fy (N x 10 ⁻¹⁰) =	0			0		
Fz (N x 10 ⁻¹⁰) =	0			0		
Mx (Nm x 10 ⁻¹⁰) =	0			0		
My (Nm x 10 ⁻¹⁰) =	0			-0.0862e-14		
Mz (Nm x 10 ⁻¹⁰) =	0			0.4596e-14		

	/dx (m)	/dy (m)	/dz (m)	/dx (m)	/dy (m)	/dz (m)
dFx (N/m x 10 ⁻¹⁰) =	26077.6	0	0	26077.58	0	0
dFy (N/m x 10 ⁻¹⁰) =	0	-13038.8	0	0	-13038.7	0
dFz (N/m x 10 ⁻¹⁰) =	0	0	-13038.8	0	0	-13038.7
dMx (Nm/m x 10 ⁻¹⁰) =	0	0	0	0	0	0
dMy (Nm/m x 10 ⁻¹⁰) =	0	0	-46.57	0	0	-46.56
dMz (Nm/m x 10 ⁻¹⁰) =	0	46.57	0	0	46.56	0

	/dθx (r)	/dθy (r)	/dθz (r)	/dθx (r)	/dθy (r)	/dθz (r)
dFx (N/rad x 10 ⁻¹⁰) =	0	0	0	0	0	0
dFy (N/rad x 10 ⁻¹⁰) =	0	0	-573.71	0	0	-573.70
dFz (N/rad x 10 ⁻¹⁰) =	0	573.71	0	0	573.70	0
dMx (Nm/rad x 10 ⁻¹⁰) =	0	0	0	0	0	0
dMy (Nm/rad x 10 ⁻¹⁰) =	0	2.049	0	0	2.048	0
dMz (Nm/rad x 10 ⁻¹⁰) =	0	0	2.049	0	0	2.048

Figure 7. Results from benchmark comparison.



	Point-to-Point			Exact to Point		
$F_x \text{ (N} \times 10^{-10}\text{)}$ =	620.274			620.274		
$F_y \text{ (N} \times 10^{-10}\text{)}$ =	0			0		
$F_z \text{ (N} \times 10^{-10}\text{)}$ =	0			0		
$M_x \text{ (Nm} \times 10^{-10}\text{)}$ =	0			0		
$M_y \text{ (Nm} \times 10^{-10}\text{)}$ =	0			-0.137e-14		
$M_z \text{ (Nm} \times 10^{-10}\text{)}$ =	0			0.137e-14		

	/dx (m)	/dy (m)	/dz (m)	/dx (m)	/dy (m)	/dz (m)
$dF_x \text{ (N/m} \times 10^{-10}\text{)}$ =	26077.6	0	0	26077.58	0	0
$dF_y \text{ (N/m} \times 10^{-10}\text{)}$ =	0	-13038.8	0	0	-13038.7	0
$dF_z \text{ (N/m} \times 10^{-10}\text{)}$ =	0	0	-13038.8	0	0	-13038.7
$dM_x \text{ (Nm/m} \times 10^{-10}\text{)}$ =	0	0	0	0	0	0
$dM_y \text{ (Nm/m} \times 10^{-10}\text{)}$ =	0	0	0	0	0	620.27
$dM_z \text{ (Nm/m} \times 10^{-10}\text{)}$ =	0	0	0	0	-620.27	0

	/dθx (r)	/dθy (r)	/dθz (r)	/dθx (r)	/dθy (r)	/dθz (r)
$dF_x \text{ (N/rad} \times 10^{-10}\text{)}$ =	0	0	0	0	-0.28e-13	0.28e-13
$dF_y \text{ (N/rad} \times 10^{-10}\text{)}$ =	0	0	-620.27	-57e-13	0	-28e-13
$dF_z \text{ (N/rad} \times 10^{-10}\text{)}$ =	0	620.27	0	57e-13	0.28e-13	0
$dM_x \text{ (Nm/rad} \times 10^{-10}\text{)}$ =	0	0	0	0	0	0
$dM_y \text{ (Nm/rad} \times 10^{-10}\text{)}$ =	0	0	0	13e-14	-13e-14	0
$dM_z \text{ (Nm/rad} \times 10^{-10}\text{)}$ =	0	0	0	13e-14	0	-13e-14

Figure 8. Results from benchmark comparison.

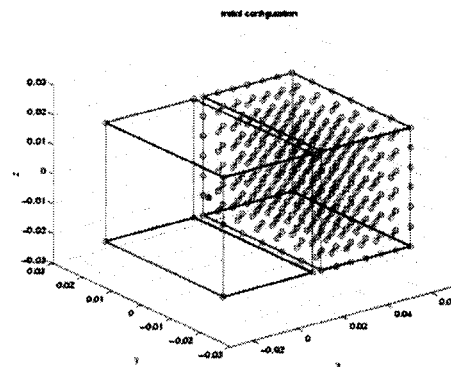


Figure 9. Grid mesh for two cubes. Proof mass in on the left.

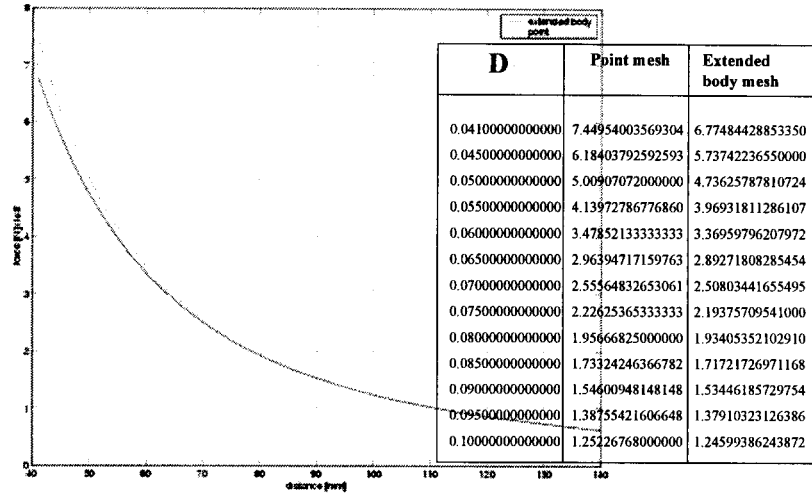


Figure 10. Comparison between point mesh and extended body mesh for two cube problem.

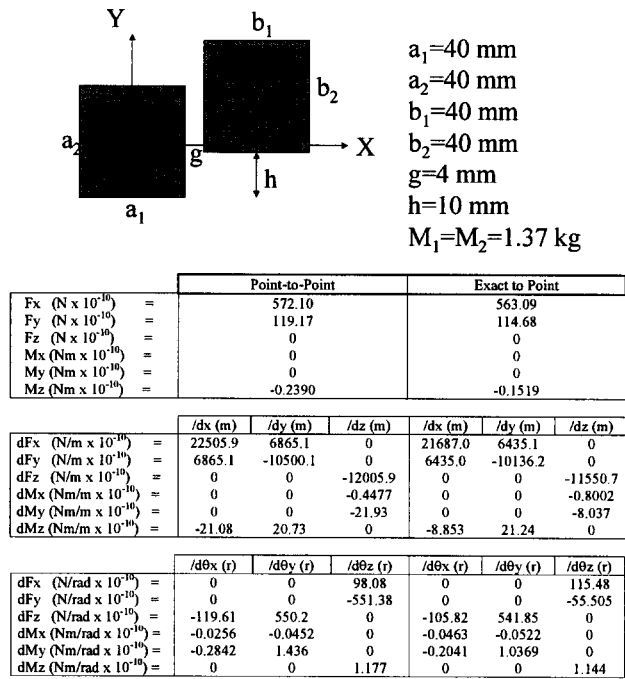


Figure 11. Results from benchmark comparison.

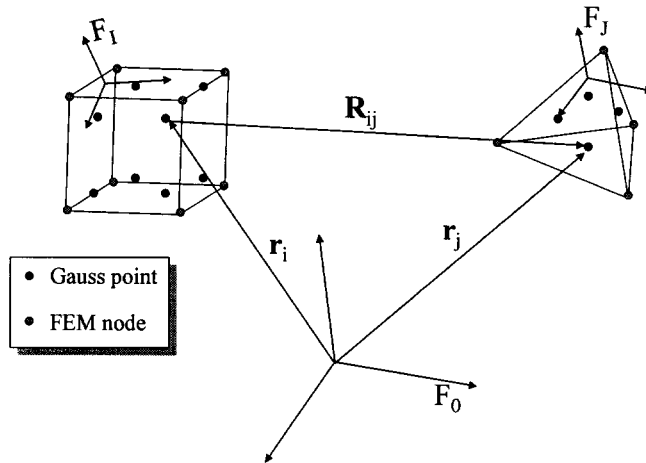


Figure 12. Summation over Gauss points belonging to separate and independent finite elements.

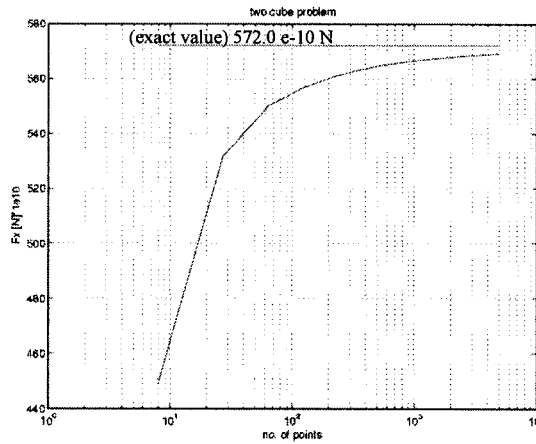


Figure 13. Axial force in two cube problem as a function of discretization points.

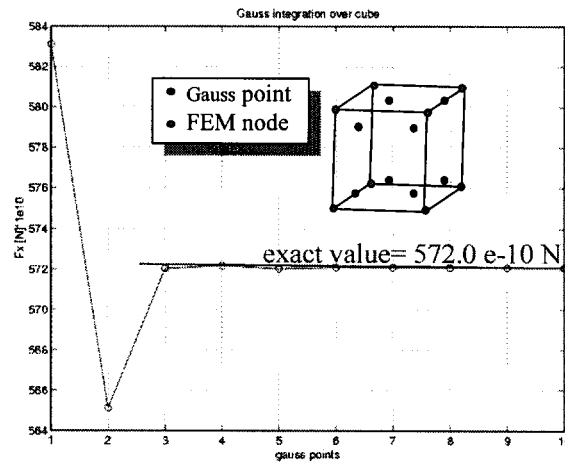
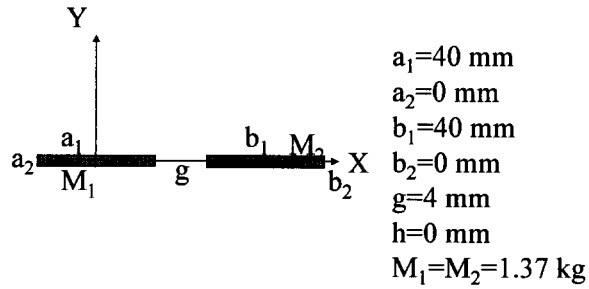


Figure 14. Axial force in two cube problem as a function of Gauss quadrature points.



	Point-to-Point			Exact to Point		
$F_x \text{ (N} \times 10^{-10}\text{)} =$	1370.37			1382.54		
$F_y \text{ (N} \times 10^{-10}\text{)} =$	0			0		
$F_z \text{ (N} \times 10^{-10}\text{)} =$	0			0		
$M_x \text{ (Nm} \times 10^{-10}\text{)} =$	0			0		
$M_y \text{ (Nm} \times 10^{-10}\text{)} =$	0			0		
$M_z \text{ (Nm} \times 10^{-10}\text{)} =$	0			0		

	$/dx \text{ (m)}$	$/dy \text{ (m)}$	$/dz \text{ (m)}$	$/dx \text{ (m)}$	$/dy \text{ (m)}$	$/dz \text{ (m)}$
$dF_x \text{ (N/m} \times 10^{-10}\text{)} =$	169,331	0	0	173,502	0	0
$dF_y \text{ (N/m} \times 10^{-10}\text{)} =$	0	-84,665	0	0	-86,753	0
$dF_z \text{ (N/m} \times 10^{-10}\text{)} =$	0	0	-84,665	0	0	-86,753
$dM_x \text{ (Nm/m} \times 10^{-10}\text{)} =$	0	0	0	0	0	0
$dM_y \text{ (Nm/m} \times 10^{-10}\text{)} =$	0	0	1177.5	0	0	1213.4
$dM_z \text{ (Nm/m} \times 10^{-10}\text{)} =$	0	-1177.5	0	0	-1213.4	0

	$/d\theta_x \text{ (r)}$	$/d\theta_y \text{ (r)}$	$/d\theta_z \text{ (r)}$	$/d\theta_x \text{ (r)}$	$/d\theta_y \text{ (r)}$	$/d\theta_z \text{ (r)}$
$dF_x \text{ (N/rad} \times 10^{-10}\text{)} =$	0	0	0	0	0	0
$dF_y \text{ (N/rad} \times 10^{-10}\text{)} =$	0	0	-2547.9	0	0	-2595.9
$dF_z \text{ (N/rad} \times 10^{-10}\text{)} =$	0	2547.9	0	0	2595.9	0
$dM_x \text{ (Nm/rad} \times 10^{-10}\text{)} =$	0	0	0	0	0	0
$dM_y \text{ (Nm/rad} \times 10^{-10}\text{)} =$	0	-33.866	0	0	-34.703	0
$dM_z \text{ (Nm/rad} \times 10^{-10}\text{)} =$	0	0	-33.866	0	0	-34.703

Figure 15. Results from benchmark comparison.

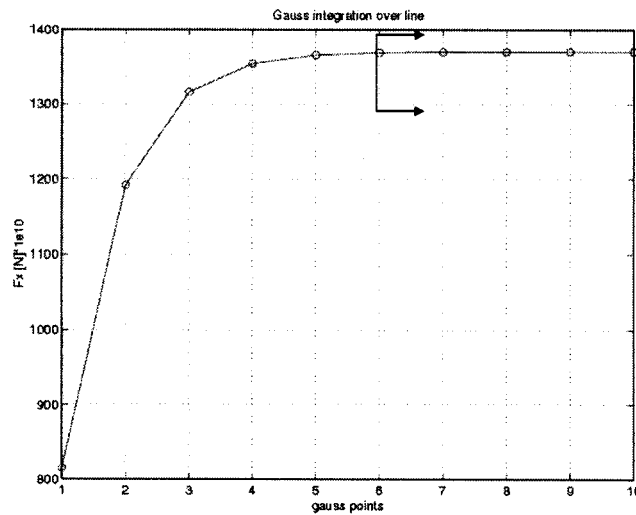
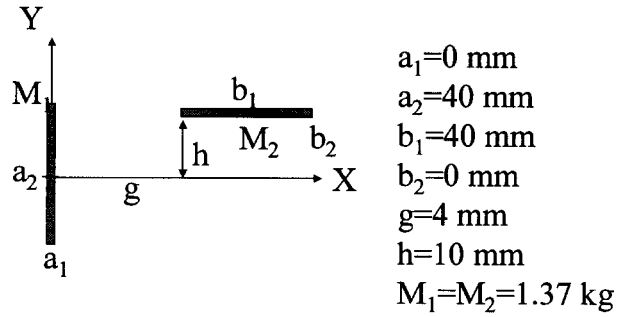


Figure 16. Axial force in two horizontal line problem as a function of Gauss quadrature points.



	Point-to-Point	Exact to Point
Fx (N x 10 ⁻¹⁰) =	2736.65	2762.18
Fy (N x 10 ⁻¹⁰) =	590.28	592.29
Fz (N x 10 ⁻¹⁰) =	0	0
Mx (Nm x 10 ⁻¹⁰) =	0	0
My (Nm x 10 ⁻¹⁰) =	0	0
Mz (Nm x 10 ⁻¹⁰) =	-18.47	-18.74

	/dx (m)	/dy (m)	/dz (m)	/dx (m)	/dy (m)	/dz (m)
dFx (N/m x 10 ⁻¹⁰) =	361645.7	44159.5	0	370131.0	44191.3	0
dFy (N/m x 10 ⁻¹⁰) =	44159.5	-65359.3	0	44191.3	-65768.8	0
dFz (N/m x 10 ⁻¹⁰) =	0	0	-296286.	0	0	-304362.
dMx (Nm/m x 10 ⁻¹⁰) =	0	0	-2372.6	0	0	-2451.3
dMy (Nm/m x 10 ⁻¹⁰) =	0	0	0	0	0	0
dMz (Nm/m x 10 ⁻¹⁰) =	-3545.8	1406.9	0	-3634.3	1432.6	0

	/dθx (r)	/dθy (r)	/dθz (r)	/dθx (r)	/dθy (r)	/dθz (r)
dFx (N/rad x 10 ⁻¹⁰) =	0	0	-2955.5	0	0	3042.6
dFy (N/rad x 10 ⁻¹⁰) =	0	0	-1329.7	0	0	-2762.1
dFz (N/rad x 10 ⁻¹⁰) =	-2962.9	2736.6	0	3042.0	1329.4	0
dMx (Nm/rad x 10 ⁻¹⁰) =	-23.73	18.47	0	-24.51	18.74	0
dMy (Nm/rad x 10 ⁻¹⁰) =	0	0	0	0	0	0
dMz (Nm/rad x 10 ⁻¹⁰) =	0	0	49.87	0	0	50.82

Figure 17. Results from benchmark comparison.

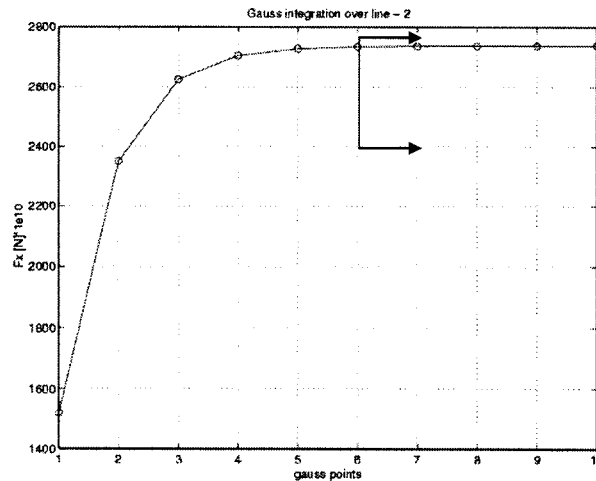


Figure 18. Axial force in two vertical lines problem as a function of Gauss quadrature points.

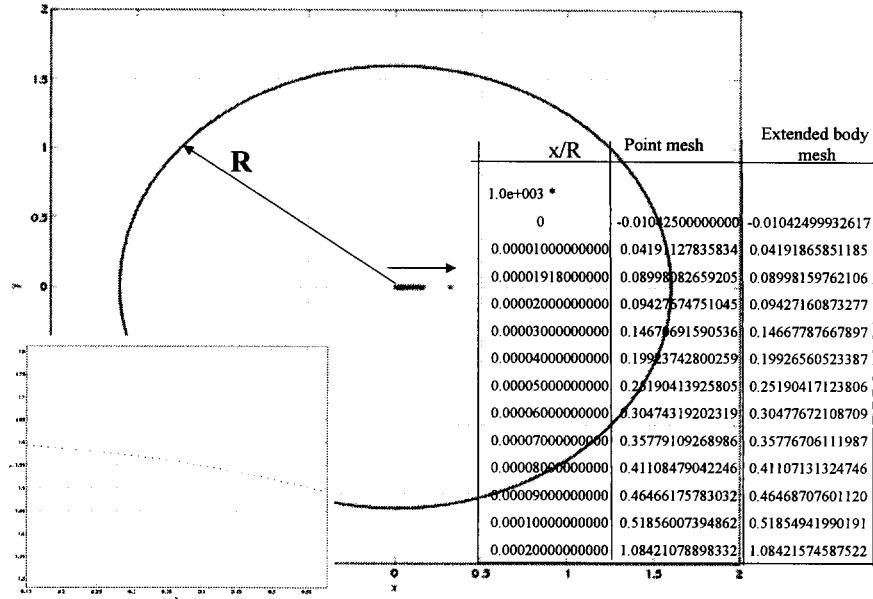


Figure 19. Results of ring mesh calculation.

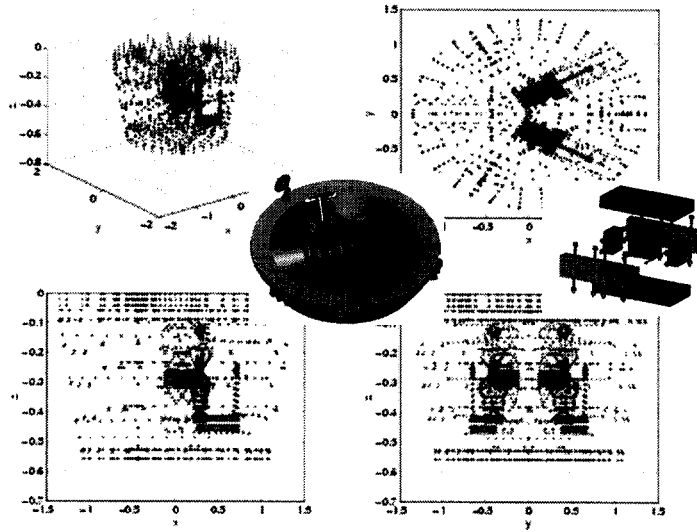


Figure 20. LISA reduced order model.

Figure 20 shows the LISA reduced order model. The model has $N=10563$ nodes for a total of 63378 degrees of freedom. The two proof masses (1.286 kg each, nodes 7 (PM # 1) and 5977 (PM # 2)) are located at

[0.07623500000000 0.29084000000000 -0.27270000000000] meters and [0.07625200000000 -0.29084000000000 -0.27270000000000] meters, respectively, in the spacecraft frame.

The proof masses are represented by point masses. Each proof mass node is connected with soft springs to a rigid element. The other end of the rigid element is attached to the side wall of the proof mass enclosure. The springs and rigid element are there to remove singularities from the model. The size of each proof mass is [50x35x35] millimeters.

Figure 21 and Figure 22 show the result of the computation. The total CPU time was 1.243 minutes (Matlab on PC).

Total CPU time: 1.243 minutes (Matlab on PC)

<p>VtotId = 2.550716464570845e-008</p> <hr/> <p>FtotId = 1.0e-008 * 0.38114392334656 -0.39563914067420 -0.39378308224236</p> <hr/> <p>dFdtotId = 1.0e-006 * 0.01292705276509 -0.32115913703691 -0.00162177859618 -0.32115913703691 0.15863546997319 -0.00913406050515 -0.00162177859618 -0.00913406050515 -0.17156252273828</p> <hr/> <p>dFdrtotId = 1.0e-006 * 0.08805634870666 -0.03666521000560 0.04841114872278 -0.00061451971287 -0.08821721134597 -0.01741700928036 0.03221601024862 -0.10167352288048 0.00016086263930</p>	<hr/> <p>MtotId = 1.0e-008 * -0.22244510347548 -0.07395540266316 -0.14221904273441</p> <hr/> <p>dMdtotId = 1.0e-006 * -0.08805634870666 0.04060304082802 -0.05236754012953 -0.00332331110956 0.08821721134597 0.01360557004690 -0.02825961884188 0.10548496211395 -0.00016086263930</p> <hr/> <p>dMdrtotId = 1.0e-007 * -0.04042100661932 0.29153977480127 0.27681120057590 0.27731787052783 -0.01515833342834 0.08771720665070 0.28420674084222 0.06547269630315 0.17009499039515</p>
---	--

Figure 21. Potential, forces, moments, and respective gradients on proof mass number 1 of the LISA reduced order model.

Vtot2d =		Mtot2d =	
2.550863331125295e-008		1.0e-008 *	
Ftot2d =		0.22786111716294	
1.0e-008 *		-0.07654283804837	
0.39089082228319		0.14667781636580	
0.41684110714230		dMdtot2d =	
-0.39270588906495		1.0e-006 *	
dFdtot2d =		0.08912476298328	0.04534584048094
1.0e-006 *		-0.00296382141953	-0.08701972972883
0.01259834140468	0.32127792090711	-0.00518323135337	0.01442813635353
0.32127792090711	0.15879867588417	-0.00702166013444	0.02811557532285
0.00518323135337	-0.00702166013444	-0.17139701728885	0.10555198119480
dFdrtot2d =		dMdrtot2d =	
1.0e-006 *		1.0e-007 *	
-0.08912476298328	-0.04141878159030	-0.04379413867454	-0.01417353041090
-0.00096323747111	0.08701972972883	-0.01833704457636	-0.29098757101974
-0.03228398639428	-0.10164307297197	0.00210503325445	0.28331403616078
			-0.27631978938316
			-0.01670236224839
			-0.08615494986654
			0.29096831996562
			-0.06336883815025
			0.17011787552566

Figure 22. Potential, forces, moments, and respective gradients on proof mass number 2 of the LISA reduced order model.

Metrics for SGT error budget determination

Once the uncertainties in mass, element displacement and element rotation are specified, the errors can be computed as follows:

- Error due to local mass uncertainty:

$$\mathcal{E}_{\Delta m} = \sum_{i=1}^N m_i \mathbf{F}(x_i, y_i, z_i) \frac{\Delta m_i}{m_i} \quad (38)$$

- Error due to total mass uncertainty:

$$\mathcal{E}_{\Delta M} = \frac{\Delta M}{M} \sum_{i=1}^N m_i \mathbf{F}(x_i, y_i, z_i) \quad (39)$$

- Error due to mass location:

$$\varepsilon_{location} = \Delta \rho \frac{\partial \mathbf{F}}{\partial (\partial^0 \rho)} \Delta \rho \quad (40)$$

- Error due to mass attitude:

$$\varepsilon_{attitude} = \Delta \theta \frac{\partial \mathbf{M}}{\partial (\partial \theta)} \Delta \theta \quad (41)$$

- Error due to proof mass attitude and location:

$$\varepsilon_{PM} = \begin{pmatrix} \Delta \rho \\ \Delta \theta \end{pmatrix}^T \begin{bmatrix} \frac{\partial \mathbf{F}}{\partial (\partial^0 \rho)} & \frac{\partial \mathbf{F}}{\partial (\partial \theta)} \\ \frac{\partial \mathbf{M}}{\partial (\partial^0 \rho)} & \frac{\partial \mathbf{M}}{\partial (\partial \theta)} \end{bmatrix}_{PM} \begin{pmatrix} \Delta \rho \\ \Delta \theta \end{pmatrix} \quad (42)$$

Survey of methods for accurate gravitational field determination

A survey of available methods for gravitational computation has been carried out, and is summarized in the following.

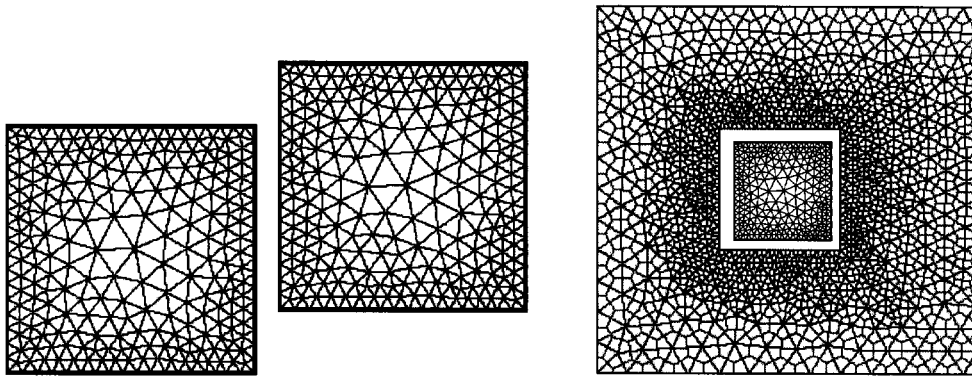


Figure 23. 2D Delaunay (simplicial) meshing for two cubes.

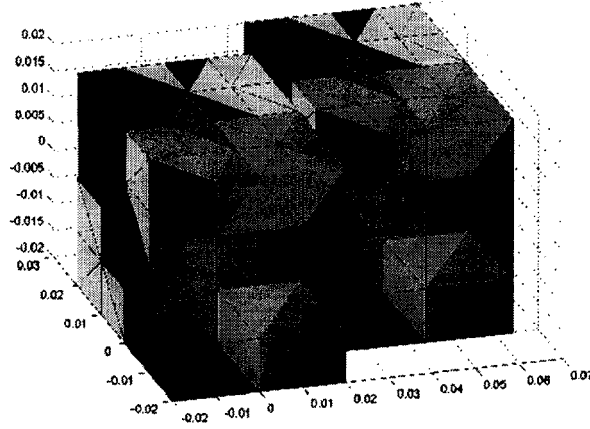


Figure 24. Two cube problem with Delaunay (simplicial) meshing.

Finite Element Method

Using a finite element approach, simplicial meshes (Delaunay and Voronoi triangulations), such as those depicted in Figure 23 are good candidates, as they follow irregularities much better than regular meshing. Figure 24 shows the two cube problem analyzed in Figure 11 but composed of a Delaunay mesh instead. In the general case, since the proof mass is a regular parallelepiped, the irregularity of the mesh around the proof mass can be modeled by tetrahedral elements with variable order of interpolation. Then we can use the SGT3 method many times over all the elements.

The solution method is based on solving the boundary value problem of Poisson's equation inside and outside the proof mass. A large spherical domain is defined which encloses the entire spacecraft. The essential (Dirichlet) boundary conditions on the outer surface of this domain are given by specifying a zero potential. The natural (Neumann) boundary conditions on the directional derivative of the potential along the surface normal are also specified to be zero (or equal to the force exerted by distance sources like the Sun, assuming the entire spacecraft is a point mass and the center of mass is fixed in the body frame).

The gravitational boundary value problem in the volume V of the domain is defined by:

- 1) the kinematic equation $\mathbf{g} = \nabla \varphi$ in V
- 2) the constitutive equation $\mathbf{q} = \frac{1}{4\pi G} \mathbf{g} = k\mathbf{g}$ in V
- 3) the balance equation $\nabla \mathbf{q} + \rho = 0$ in V
- 4) the potential boundary condition $\varphi = \hat{\varphi}$ on S_u
- 5) the force boundary condition $\mathbf{q}_n = \mathbf{q} \cdot \mathbf{n} = \hat{\mathbf{q}}$ on S_q

where \mathbf{g} is the gradient of the potential φ , \mathbf{n} is the outer normal to V , ρ is the local material density, and the caret denotes prescribed boundary conditions on the potential and the vector \mathbf{q} on the surfaces S_u and S_q respectively.

The variational statement of the boundary value problem can be written as

$$\delta\pi = \int_V [k\nabla\varphi \cdot \delta\nabla\varphi - \rho\delta\varphi]dV - \int_{S_q} \hat{\mathbf{q}}\delta\varphi dS = 0 \quad (43)$$

Introducing the shape functions \mathbf{N} , the potential and the density can be interpolated as

$$\begin{aligned}
 \varphi &= \mathbf{N}(x, y, z) \mathbf{p} \\
 \delta\varphi &= \mathbf{N}(x, y, z) \delta\mathbf{p} \\
 \nabla\varphi &= \nabla\mathbf{N}(x, y, z) \mathbf{p} \\
 \delta\nabla\varphi &= \nabla\mathbf{N}(x, y, z) \delta\mathbf{p} \\
 \nabla\nabla\varphi &= \nabla \otimes \nabla\mathbf{N}(x, y, z) \mathbf{p}
 \end{aligned}
 \tag{44}$$

Substituting in the variational statement, we obtain

$$\begin{aligned}
 \mathbf{k}\mathbf{p} &= \mathfrak{M} \\
 \mathbf{k} &= \int_V [\nabla\mathbf{N}^T \mathbf{k} \mathbf{1}_{n \times n} \nabla\mathbf{N}] dV \\
 \mathfrak{M} &= \int_V \mathbf{N}^T \rho(x, y, z) dV + \int_{S_q} \mathbf{N}^T \hat{\mathbf{q}} dS
 \end{aligned}
 \tag{45}$$

We can see that to get at least a constant force gradient estimation within an element, we need a quadratic shape function at least. Therefore, this method leads to higher order interpolating functions. The advantage, however, is that a coarser grid can be used far away from the proof mass, with a finer mesh in close proximity to the proof mass.

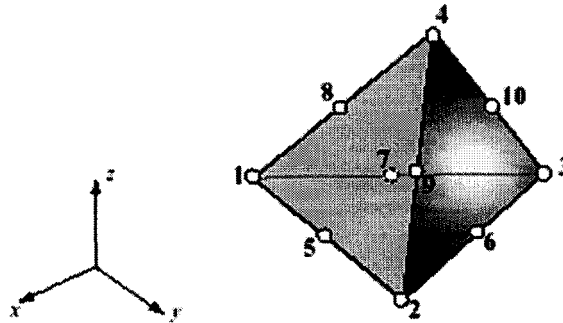


Figure 25. Ten node tetrahedron.

Figure 25 shows the nodal configuration of an isoparametric tetrahedral element. The interpolation scheme is as follows:

$$w = [w_1 \quad w_2 \quad w_3 \quad w_4 \quad w_5 \quad w_6 \quad w_7 \quad w_8 \quad w_9 \quad w_{10}] \begin{bmatrix} \xi_1 (2\xi_1 - 1) \\ \xi_2 (2\xi_2 - 1) \\ \xi_3 (2\xi_3 - 1) \\ \xi_4 (2\xi_4 - 1) \\ 4\xi_1\xi_2 \\ 4\xi_2\xi_3 \\ 4\xi_3\xi_1 \\ 4\xi_1\xi_4 \\ 4\xi_2\xi_4 \\ 4\xi_3\xi_4 \end{bmatrix} \quad (46)$$

where, for a point located at (x,y,z),

$$\begin{pmatrix} \xi_1 \\ \xi_2 \\ \xi_3 \\ \xi_4 \end{pmatrix} = \frac{1}{6V} \begin{bmatrix} 6V_1 & a_1 & b_1 & c_1 \\ 6V_2 & a_2 & b_2 & c_2 \\ 6V_3 & a_3 & b_3 & c_3 \\ 6V_4 & a_4 & b_4 & c_4 \end{bmatrix} \begin{pmatrix} 1 \\ x \\ y \\ z \end{pmatrix} \quad (47)$$

Finite difference method

Another method to determine the gravitational potential over the mass distribution is to obtain the local mass density at element level from NASTRAN and solve Poisson's equation over a surrounding domain. The discretized Poisson's equation in 3D finite differences becomes:

$$\begin{aligned} \nabla^2 \varphi &\approx \\ \varphi_{i-1,j,k} + \varphi_{i+1,j,k} + \varphi_{i,j-1,k} + \varphi_{i,j+1,k} + \varphi_{i,j,k-1} + \varphi_{i,j,k+1} - 6\varphi_{i,j,k} & \\ = 4\pi G \rho_{i,j,k} & \end{aligned} \quad (48)$$

where $\varphi_{i,j,k}$ and $\rho_{i,j,k}$ are the discretized potential and the discretized density at (i,j,k) , respectively. This is a 7-point template to discretize the Laplacian operator. This discretization results in a large system of linear equations relating the unknown grid point potentials to the known right-hand side density distribution. This system of equations can be solved efficiently using FFT.

In the Fourier space, the Poisson's equation is

$$\bar{\varphi}(\mathbf{k}) = \bar{G}(\mathbf{k}) \bar{\rho}(\mathbf{k}) \quad (49)$$

where $\mathbf{k} = (k_x, k_y, k_z)$ is the wave number with $k_x = 2\pi l/L$, $k_y = 2\pi m/L$, $k_z = 2\pi n/L$ for component (l,m,n) and box size L , and $\bar{G}(\mathbf{k})$ is the Green's function which for the adopted discretization is equal to:

$$\bar{G}(\mathbf{k}) = -4\pi G \left[\sin^2\left(\frac{k_x}{2}\right) + \sin^2\left(\frac{k_y}{2}\right) + \sin^2\left(\frac{k_z}{2}\right) \right]^{-1} \quad (50)$$

The procedure is then:

- a) perform FFT to get the transformed potential and density fields,
- b) solve the system of equations $\bar{\varphi}_{i,j,k} = \bar{G}(\mathbf{k}_{i,j,k}) \bar{\rho}_{i,j,k}$,
- c) do inverse FFT to recover the physical fields,
- d) compute forces at each grid node from $f_{i,j,k}^x = -(\varphi_{i+1,j,k} - \varphi_{i-1,j,k})/2$ etc.

A more efficient discretization is achieved using a space-centering approach.

Fast Multipole Expansion

To extend the models to include the capability for handling inhomogeneity and assist with gravitational balancing, another solution is the fast multipole expansion. Following previous work done in this area [5], it seems that a fast multipole expansion is one of the best choices to avoid expensive and possibly inaccurate numerical integration over irregular domains. In addition, the fact that an exact representation exists for the potential of a mass distribution allows knowing ahead of time the truncation error of the series, so that different accuracy can be assigned to different domains of solution. The gravitational potential energy of a test mass, with density distribution of $\rho(\mathbf{x}')$ at \mathbf{x}' , in a gravitational potential due to a source mass with a density distribution $\rho(\mathbf{x})$ at \mathbf{x} is given by:

$$\varphi = -4\pi G \sum_{l=0}^{\infty} \frac{1}{2l+1} \sum_{m=-l}^{+l} q_{lm} Q_{lm} \quad (51)$$

where the multipole moments

$$q_{lm} = \int \rho(\mathbf{x}') r'^l Y_{lm}^*(\theta', \phi') d\mathbf{x}' \quad (52)$$

and the multipole fields

$$Q_{lm} = \int \rho(\mathbf{x}) r^{-(l+1)} Y_{lm}(\theta, \phi) d\mathbf{x} \quad (53)$$

are integrated over the test mass and the source, respectively. Here, Y_{lm} are spherical harmonics. As an example, the 0-th order term is

$$\varphi = -4\pi G q_{00} Q_{00} \quad (54)$$

with

$$q_{00} = \int \rho(\mathbf{x}') Y_{00}^*(\theta', \phi') d\mathbf{x}' \quad (55)$$

$$Q_{00} = \int \rho(\mathbf{x}) r^{-1} Y_{00}(\theta, \phi) d\mathbf{x} \quad (56)$$

and Y_{00} are spherical harmonic coefficients.

Assuming q_{lm} and Q_{lm} are known at about a coordinate origin O, they can be expressed about a generic point P(r', θ', ϕ') as:

$$\begin{aligned} \tilde{q}_{LM} = & \sum_{l', m', l, m} \sqrt{\frac{4\pi(2L+1)!}{(2l'+1)!(2l+1)!}} \times \\ & r'^{l'} Y_{l', m'}^*(r') C(l', m', l, m, L, M) \delta_{L, l+l'} q_{lm} \end{aligned} \quad (57)$$

and

$$\begin{aligned} \tilde{Q}_{LM} = & \sum_{l', m', l, m} \sqrt{\frac{4\pi(2l)!}{(2L+1)!(2l'+1)!}} \times \\ & r'^{l'} Y_{l', m'}(r') C(l', m', l, m, L, M) \delta_{L, l+l'} Q_{lm} \end{aligned} \quad (58)$$

where $C(\cdot)$ are Clebsch-Gordon coefficients.

The gradients can be computed analytically by differentiating the potential with respect to the radius r' and the azimuth θ' and elevation ϕ' .

This paper has described the development of the self-gravity tool used to predict and control the motion of one of the proof masses of the orbiting LISA gravitational wave detector. Three computational models have been described. First, a model using summation over point masses. Second, a model using the exact solution obtained for a uniform parallelepiped and a point mass. Third, a more general finite element model capable of directly using NASTRAN mesh information for arbitrarily complex geometries. The capabilities of these computational engines have been demonstrated with some numerical examples, including a realistic mesh of the LISA spacecraft.

Acknowledgement This research was performed at the Jet Propulsion Laboratory, California Institute of Technology, under contract with the National Aeronautics and Space Administration. The author is grateful to the LISA Project for a very scientifically stimulating environment, and to William Haile of Swales Aerospace for providing a way to check some of the calculations presented in this paper.

References:

1. Kane, Likins, Levinson, *Spacecraft Dynamics*, McGraw-Hill, 1982.
2. McMillan, *The Theory of the Potential*, Dover, 1930.
3. Quadrelli M.B., Hadaegh, F.Y., Singh, G., and Shields, J.F.: *Some observations on the Dynamics and Control of Spacecraft Formations*, presented at the IFAC Conference on Aerospace Controls, Bologna, Italy, September 2-7, 2001.
4. Vitale, S.: *Gravitational Field Compensation*, LISA Technology Package Architect Document, Unitn-Int-4-2001 Report from the University of Trento, Italy.
5. D'Urso, C., and Adelberger, E.G.: *Translation of multipoles for a $1/r$ potential*, Physical review D, vol. 55, no.12, June 1997, 7970-2.